PNAS RESEARCH ARTICLE | NEUROSCIENCE OPEN ACCESS

Morphological, cellular, and molecular basis of brain infection in COVID-19 patients

Fernanda Crunfli[a,1], Victor C. Carregari[a,1], Flavio P. Veras[b,1], Lucas S. Silva[a], Mateus Henrique Nogueira[a], André Saraiva Leão Marcelo Antunes[a], Pedro Henrique Vendramini[a], Aline Gazzola Fragnani Valença[a], Caroline Brandão-Teles[a], Giuliana da Silva Zuccoli[a], Guilherme Reis-de-Oliveira[a], Lícia C. Silva-Costa[a], Verônica Monteiro Saia-Cereda[a], Bradley J. Smith[a], Ana Campos Codo[a], Gabriela F de Souza[a], Stéfanie P. Muraro[a], Pierina Lorencini Parise[a], Daniel A. Toledo-Teixeira[a], Ícaro Maia Santos de Castro[c], Bruno Marcel Melo[b], Glaucia M. Almeida[b], Egidi Mayara Silva Firmino[b], Isadora Marques Paiva[b], Bruna Manuella Souza Silva[b], Rafaela Mano Guimarães[b], Niele D. Mendes[b], Raíssa L. Ludwig[a], Gabriel P. Ruiz[a], Thiago L. Knittel[a], Gustavo G. Davanzo[a], Jaqueline Aline Gerhardt[a], Patrícia Brito Rodrigues[a], Julia Forato[a], Mariene Ribeiro Amorim[a], Natália S. Brunetti[a], Matheus Cavalheiro Martini[a], Maíra Nilson Benatti[b], Sabrina S. Batah[b], Li Siyuan[b], Rafael B. João[a], Ítalo K. Aventurato[a], Mariana Rabelo de Brito[a], Maria J. Mendes[a], Beatriz A. da Costa[a], Marina K. M. Alvim[a], José Roberto da Silva Júnior[a], Lívia L. Damião[a], Iêda Maria P. de Sousa[a], Elessandra D. da Rocha[a], Solange M. Gonçalves[a], Luiz H. Lopes da Silva[a], Vanessa Bettini[a], Brunno M. Campos[a], Guilherme Ludwig[a], Lucas Alves Tavares[b], Marjorie Cornejo Pontelli[b], Rosa Maria Mendes Viana[b], Ronaldo B. Martins[b], Andre Schwambach Vieira[a], José Carlos Alves-Filho[b], Eurico Arruda[b], Guilherme Gozzoli Podolsky-Gondim[b], Marcelo Volpon Santos[b], Luciano Neder[b], André Damasio[a], Stevens Rehen[d,e], Marco Aurélio Ramirez Vinolo[a], Carolina Demarchi Munhoz[c], Paulo Louzada-Junior[b], Renê Donizeti Oliveira[b], Fernando Q. Cunha[b], Helder I. Nakaya[c], Thais Mauad[c], Amaro Nunes Duarte-Neto[c], Luiz Fernando Ferraz da Silva[c], Marisa Dolhnikoff[c], Paulo Hilario Nascimento Saldiva[c], Alessandro S. Farias[a], Fernando Cendes[a], Pedro Manoel M. Moraes-Vieira[a], Alexandre T. Fabro[b], Adriano Sebollela[b], José L. Proença-Modena[a], Clarissa L. Yasuda[a,2], Marcelo A. Mori[a,2], Thiago M. Cunha[b,2], and Daniel Martins-de-Souza[a,d,2]

Edited by Marcus Raichle, Washington University in St. Louis, St. Louis, MO; received January 26, 2022; accepted June 15, 2022

Although increasing evidence confirms neuropsychiatric manifestations associated mainly with severe COVID-19 infection, long-term neuropsychiatric dysfunction (recently characterized as part of "long COVID-19" syndrome) has been frequently observed after mild infection. We show the spectrum of cerebral impact of severe acute respiratory syndrome coronavirus 2 (SARS-CoV-2) infection, ranging from long-term alterations in mildly infected individuals (orbitofrontal cortical atrophy, neurocognitive impairment, excessive fatigue and anxiety symptoms) to severe acute damage confirmed in brain tissue samples extracted from the orbitofrontal region (via endonasal transethmoidal access) from individuals who died of COVID-19. In an independent cohort of 26 individuals who died of COVID-19, we used histopathological signs of brain damage as a guide for possible SARS-CoV-2 brain infection and found that among the 5 individuals who exhibited those signs, all of them had genetic material of the virus in the brain. Brain tissue samples from these five patients also exhibited foci of SARS-CoV-2 infection and replication, particularly in astrocytes. Supporting the hypothesis of astrocyte infection, neural stem cell–derived human astrocytes in vitro are susceptible to SARS-CoV-2 infection through a noncanonical mechanism that involves spike–NRP1 interaction. SARS-CoV-2–infected astrocytes manifested changes in energy metabolism and in key proteins and metabolites used to fuel neurons, as well as in the biogenesis of neurotransmitters. Moreover, human astrocyte infection elicits a secretory phenotype that reduces neuronal viability. Our data support the model in which SARS-CoV-2 reaches the brain, infects astrocytes, and consequently, leads to neuronal death or dysfunction. These deregulated processes could contribute to the structural and functional alterations seen in the brains of COVID-19 patients.

SARS-CoV-2 | COVID-19 | neurological symptoms | astrocytes | NRP1

Significance

Neurological symptoms are among the most prevalent of the extrapulmonary complications of COVID-19, affecting more than 30% of patients. In this study, we provide evidence that severe acute respiratory syndrome coronavirus 2 (SARS-CoV-2) is found in the human brain, where it infects astrocytes and to a lesser extent, neurons. We also show that astrocytes are susceptible to SARS-CoV-2 infection through a noncanonical mechanism that involves spike–NRP1 interaction and respond to the infection by remodeling energy metabolism, which in turn, alters the levels of metabolites used to fuel neurons and support neurotransmitter synthesis. The altered secretory phenotype of infected astrocytes then impairs neuronal viability. These features could explain the damage and structural changes observed in the brains of COVID-19 patients.

COVID-19 is a disease caused by infection with severe acute respiratory syndrome coronavirus 2 (SARS-CoV-2). Although the hallmark symptoms of COVID-19 are respiratory in nature and related to pulmonary infection, extrapulmonary effects have been reported in COVID-19 patients (1, 2), including symptoms involving the central nervous system (CNS) (3). Notably, over 30% of hospitalized COVID-19 patients manifest neurological and even neuropsychiatric symptoms (4, 5), and some present varying degree of encephalitis (6). There are increasing reports of persistent and prolonged effects after acute COVID-19, a long COVID-19 syndrome characterized by persistent symptoms and/or delayed or long-term complications beyond 4 wk from the onset of symptoms. Some of these persistent symptoms are neuropsychiatric sequelae (3). One study revealed that more than half of hospitalized patients continued to exhibit neurological symptoms for as long as 3 mo after the acute stage (7). Impaired cognition has also been

This article is a PNAS Direct Submission.

Published August 11, 2022.

confirmed in recovered patients after hospitalization (8–11), and neurological impairment is consistent with substantial damage to the nervous system (12). Previous studies on severe acute respiratory syndrome (SARS) patients reported the presence of the SARS coronavirus in the brain tissue and cerebrospinal fluid of subjects who presented neurological symptoms (13–15). SARS-CoV-2 RNA was also detected in the cerebrospinal fluid of patients with meningitis (16–18). Moreover, alterations in the cerebral cortical region compatible with viral infection (19), a loss of white matter, and axonal injury (20) have all been reported in COVID-19 patients.

In line with the potential neurotropic properties of SARS-CoV-2, recent evidence indicated the presence of viral proteins in brain regions of COVID-19 patients (21, 22) as well as in the brains of K18-ACE2 transgenic mice (22, 23) and Syrian hamsters (24) infected with SARS-CoV-2. The presence of SARS-CoV-2 in the human brain has been associated with marked astrogliosis, microgliosis, and immune cell accumulation (21). Further indicating the ability of SARS-CoV-2 to infect cells of the CNS, SARS-CoV-2 has also been shown to infect human brain organoid cells in culture (22, 25–27). Recently, SARS-CoV-2 has been found to cross the blood–brain barrier (BBB) in mice (28–30) and in two-dimensional static and three-dimensional microfluidic in vitro models (31, 32), therefore potentially reducing the integrity of the BBB.

Despite the accumulating evidence, an integrated understanding of the cellular and molecular mechanisms involved in SARS-CoV-2 brain infection and the consequent repercussions on brain structure and functionality is lacking. To gain further insight into the neuropathological and neurological consequences of COVID-19 and possible cellular and molecular mechanisms, we performed a broad translational investigation of living patients, postmortem brain samples, and preclinical in vitro and ex vivo models. Clinical data and brain imaging features of COVID-19 patients were found to be associated with neuropathological and biochemical changes caused by SARS-CoV-2 infection in the CNS. We found that astrocytes are the main sites of viral infection within the CNS. SARS-CoV-2–infected astrocytes exhibited marked metabolic changes resulting in a reduction of the metabolites used to fuel neurons and build neurotransmitters. Infected astrocytes were also found to secrete unidentified factors that lead to neuronal death. These events could contribute to the neuropathological alterations, neuropsychiatric symptoms, and cognitive impairment observed in COVID-19 patients.

Results

Cognitive Impairments and Neuropsychiatric Symptoms in Convalescent COVID-19 Patients Correlate with Altered Cerebral Cortical Thickness. We performed a cortical surface–based morphometry analysis (using a high-resolution 3T MRI) on 81 subjects diagnosed with mild COVID-19 infection (62 self-reported anosmia or dysgeusia) who did not require oxygen support (methodological details and patient demographics are presented in *SI Appendix*). The analysis was performed within an average (SD) interval of 57 (26) d after SARS-CoV-2 detection by qRT-PCR, and the subjects were compared with 81 healthy volunteers (without neuropsychiatric comorbidities) scanned during the COVID-19 pandemic (balanced for age [$P = 0.97$] and sex [$P = 0.3$]). The COVID-19 group presented higher levels of anxiety and depression symptoms, fatigue, and excessive daytime sleepiness (*SI Appendix*, Table S1 shows epidemiological and clinical data). An analysis of cortical thickness (adjusted for multiple comparisons using the Holm–Bonferroni method) revealed areas of reduced cortical thickness exclusively in the left hemisphere, including the left gyrus rectus ($P = 0.01$), superior temporal gyrus ($P = 0.036$), inferior temporal sulcus ($P = 0.02$), and posterior transverse collateral sulcus ($P = 0.003$) (Fig. 1*A*). There was no observed increase in cortical thickness.

A subgroup of 61 participants of the COVID-19 group also underwent neuropsychological evaluation, which assessed episodic verbal memory (logical memory subtest, immediate and delayed recall, Wechsler Memory Scale), sustained attention (Color Trails A), and alternating attention and cognitive flexibility (Color Trails B). The tests were performed a median of 59 d (range between 21 and 120 d) after diagnosis; we observed fatigue in ∼70% of individuals and daytime sleepiness in 36%. Despite the high level of education of the participant subgroup (median of 16 y), the comparisons with Brazilian normative data (z scores were adjusted for age, sex, and education) showed that nearly 28% of participants presented impairments (z scores ≤ -1) in immediate episodic verbal memory (immediate recall, including mild, moderate, and severe impairments), and ∼34 and 56% underperformed (z scores ≤ -1) on Color Trails A (sustained attention) and B (alternating attention and cognitive flexibility), respectively (*SI Appendix*, Fig. S1 and Table S2). Interestingly, 77% of these COVID-19 patients also presented acute anosmia or dysgeusia, which may be related to the observed changes in cortical thickness (19). The high proportions of anosmia and dysgeusia support the idea of the virus entering the nervous system, more specifically the orbitofrontal region (due to the proximity and communication with the nasal cavity).

We observed a negative correlation between BAI (Beck Anxiety Inventory) scores and the cortical thickness of orbitofrontal regions (adjusted for fatigue scores) (Fig. 1*B* and *SI Appendix*, Table S3). We also identified a positive correlation between immediate episodic verbal memory and cortical thickness of regions associated with language (adjusted for fatigue scores) (Fig. 1*C* and *SI Appendix*, Table S3). There was a likely correlation between Color Trail B and the thickness of the gyrus rectus after adjusting for fatigue ($r = 0.2$, $P = 0.13$). Our findings indicate that cortical thickness atrophy is associated with neuropsychiatric symptoms and cognitive impairment in COVID-19 patients with mild or no respiratory symptoms.

SARS-CoV-2 Infects and Replicates in Human Brain Astrocytes of COVID-19 Patients. Brain alterations in COVID-19 patients are hypothesized to be a consequence of either inflammatory or hemodynamic changes secondary to peripheral infection or a consequence of SARS-CoV-2 invading the CNS and compromising cell viability and brain function. Although exacerbated inflammation and cardiovascular dysfunction have been well characterized in COVID-19 patients who progress to the severe stages of the disease (33), the molecular and cellular underpinnings of SARS-CoV-2 CNS infection remain elusive. We performed a minimally invasive autopsy via endonasal transethmoidal access to obtain brain samples from 26 individuals who died of COVID-19. It is worth mentioning that these samples were from brain regions in close proximity to the areas in which we identified altered cortical thickness in the patients of the cohort evaluated noninvasively by MRI.

An unbiased histopathological analysis revealed alterations consistent with necrosis and inflammation in 5 of 26 brain tissue samples (*SI Appendix*, Tables S4 and S5). A deeper analysis of these five samples revealed a strong predominance of senile changes, such as corpora amylacea, lipofuscin deposits, and parenchymal retraction around the vessels and the meninges. Due to the type of collection performed, alternating white and

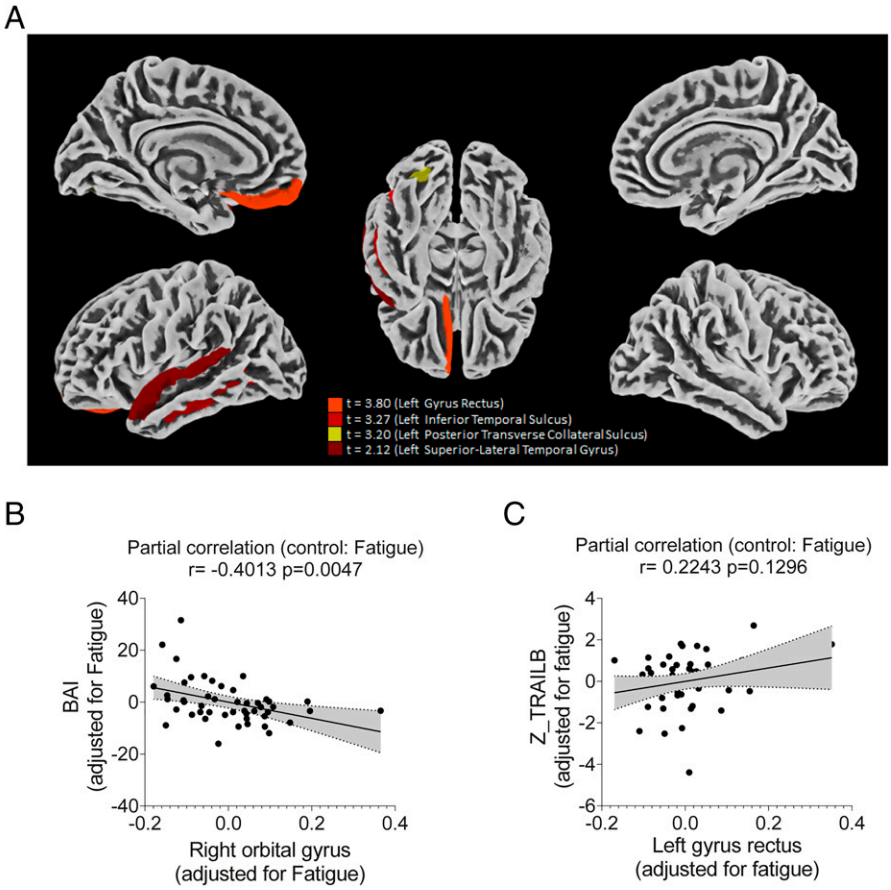

Fig. 1. Cortical thickness atrophy after mild COVID-19 infection. Surface-based morphometry by high-resolution 3T MRI (*A*). Results from the analysis of 81 subjects with confirmed SARS-CoV-2 diagnosis (who had mild respiratory symptoms and did not require hospitalization or oxygen support) compared with 81 healthy volunteers (without a diagnosis of COVID-19). The analysis was performed within an average (SD) of 57.23 (25.91) d after diagnosis. (*B*) Correlation between anxiety scores (BAI) and right orbital gyrus thickness. (*C*) Correlation between Color Trail B test (Z-TRAILB: z-scores were based on Brazilian normative data) and left gyrus rectus thickness. Data depict partial correlation coefficients (adjusted for fatigue).

gray matter was observed. Intraparenchymal inflammatory processes were minimal but present, represented by lymphocytes and perivascular microglia proliferation. In two cases, more intense inflammation was observed, represented by tiny inflammatory aggregates associated with endothelial hyperplasia or gemistocytic astrocytes. Cases with nasal epithelium sampled together with brain puncture demonstrated adaptive epithelial changes with cell ballooning of the most superficial cells. Moreover, small, multifocal areas of liquefaction necrosis were observed (Fig. 2*A* and *SI Appendix*, Fig. S2*A*).

Hypothesizing that the histopathological signs of brain damage would guide us to SARS-CoV-2 brain infection, we evaluated the presence of SARS-CoV-2 in the five brain samples that presented histopathological alterations (*SI Appendix*, Tables S4 and S5). SARS-CoV-2 genetic material and spike protein were detected in all five samples (Fig. 2 *B* and *C*). On average, SARS-CoV-2 spike protein was detected in 37% of the cells in the brain tissue (Fig. 2*D*). The majority of these SARS-CoV-2 spike-positive cells (65.93%) were astrocytes (glial fibrillary acidic protein positive [GFAP+] cells) (Fig. 2*E* and *SI Appendix*, Fig. S2*B*). Considering that only 18.52% of all brain cells on the slides were GFAP+, our results indicate that SARS-CoV-2 preferentially infects astrocytes. We also detected SARS-CoV-2 spike protein in neurons, although to a lesser extent (NeuN+ cells) (Fig. 2*E* and *SI Appendix*, Fig. S3*A*). We did not find signs of infection in microglia (Iba-1+ cells) (Fig. 2*E* and *SI Appendix*, Fig. S3*B*). The specificity of antispike antibodies was validated in the brain tissue of COVID-19–free cases and in SARS-CoV-2–infected Vero cells (*SI Appendix*, Fig. S4). Additionally, the presence of SARS-CoV-2 spike protein was directly correlated with the presence of double-stranded RNA (dsRNA) in the cells (Fig. 2*C* and *SI Appendix*, Fig. S3*C*), an indicator of replicative viruses in the brain tissue (34). The relative number of brain cell subtypes in our samples is shown in *SI Appendix*, Fig. S3*D* (*SI Appendix*).

To confirm that SARS-CoV-2 infects human brain cells, we analyzed brain slices from human cortices that were exposed to SARS-CoV-2. Both SARS-CoV-2 spike protein and dsRNA were detected in human brain slices 48 h postinfection (hpi) (*SI Appendix*, Fig. S5*A*), and the SARS-CoV-2 gene was detected by RT-PCR of the nucleocapsid N1 transcript at both 24 and 48 hpi (*SI Appendix*, Fig. S5*B*). SARS-CoV-2 astrocyte infection was confirmed by immunostaining the SARS-CoV-2 spike protein and GFAP (*SI Appendix*, Fig. S5*C*). We observed that the majority of the spike-positive cells (comprising 5.65% of the total cells) were positive for GFAP (58.33% of infected cells) (*SI Appendix*, Fig. S5*D*), similar to the percentage of infected astrocytes observed in the five histologically altered postmortem samples. The relative number of brain cell subtypes in our samples is shown in *SI Appendix*, Fig. S5*E* (*SI Appendix*). These data indicate that in the CNS, SARS-CoV-2 preferentially infects astrocytes and replicates within them, in line with the human postmortem brain findings.

To investigate proteome-level changes caused by SARS-CoV-2 infection, we conducted a liquid chromatography–mass spectrometry (LC/MS) proteomic analysis with a separate set of samples

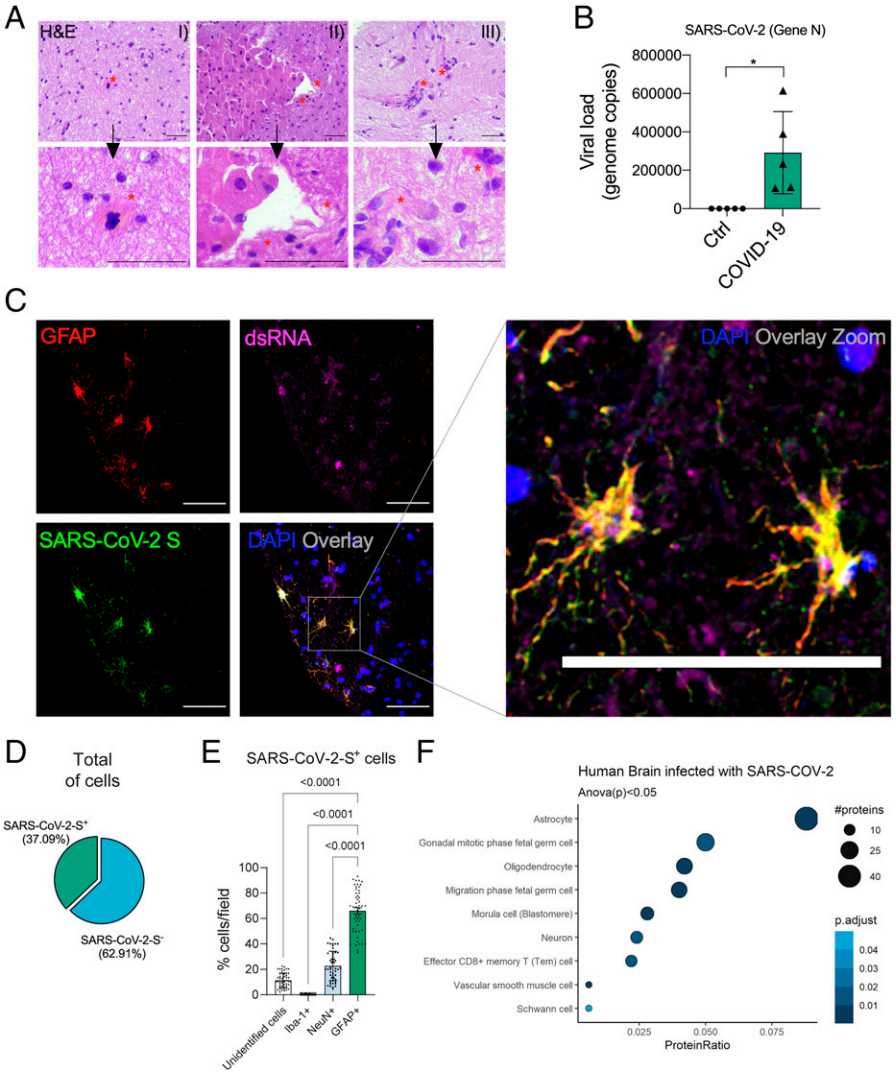

Fig. 2. SARS-CoV-2 infects the CNS, replicates in astrocytes, and causes brain damage. (*A*) Histopathological H&E images of postmortem brain tissue from individuals who died of COVID-19. Five of 26 individuals showed signs of brain damage as represented in the images by (*A*, *I*) areas of necrosis, cytopathic damage (i.e., enlarged, hyperchromatic, atypical-appearing nuclei), (*A*, *II*) vessels with margination of leukocytes and thrombi, and (*A*, *III*) an infiltration of immune cells. The alterations are indicated by red asterisks and respective zoomed-in images (*Lower*). Images were acquired with 400× magnification. (Scale bars: 50 μm.) (*B*) Viral load in brain tissues from the five COVID-19 patients who manifested histopathological alterations in the brain as compared with samples from SARS-CoV-2–negative controls ($n = 5$ per group). *$P < 0.05$ compared with the control group. (*C*) Representative confocal images of the brain tissue of one COVID-19 patient who manifested histopathological alterations. Immunofluorescence targeting GFAP (red), dsRNA (magenta), SARS-CoV-2-S (green), and nuclei (DAPI; blue). Images were acquired with 630× magnification. (Scale bars: 50 μm.) (*D*) Percentage of SARS-CoV-2-S–positive cells in the tissue of the five COVID-19 patients. (*E*) Percentage of GFAP+ vs. unidentified cells, Iba1+, and NeuN+ among all infected cells. Ten fields/cases were analyzed. (*F*) Cell type enrichment analysis using the dataset generated from postmortem brain tissue from patients who died of COVID-19. Dot size represents the number of proteins related to the respective cell type, and the color represents the *P* value adjusted by false discovery rate. All data are shown as mean ± SEM. *P* values were determined by two-tailed unpaired tests with Welch's correction (*B*) or ANOVA one way followed by Tukey's post hoc test (*E*). H&E: hematoxylin and eosin; DAPI: 4′,6-diamidino-2-phenylindole.

consisting of 12 postmortem brain samples from COVID-19 patients vs. 8 SARS-CoV-2–negative controls (*SI Appendix*, Tables S6 and S7). We identified 656 differentially expressed proteins: 117 down-regulated and 539 up-regulated. Pathways associated with neurodegenerative diseases, carbon metabolism, and oxidative phosphorylation were enriched among the differentially expressed proteins (*SI Appendix*, Fig. S6). Notably, proteins expressed in astrocytes were enriched among the differentially expressed proteins, consistent with the higher frequency of infected astrocytes observed in COVID-19 postmortem brains (Fig. 2*F*).

To gather further evidence of the susceptibility of human astrocytes to SARS-CoV-2 infection, neural stem cell–derived human astrocytes (BR-1 cell line) (35) were exposed to the virus, and the viral load was determined at 24 hpi (Fig. 3*A*). Confirming what was seen in the postmortem brain samples, viral genetic material (Fig. 3*B*), dsRNA, and spike protein (Fig. 3 *C* and *D*) were detected in infected cells with significant overlap (Fig. 3 *C* and *E*). SARS-CoV-2 infection reduces cell viability by over 25% at 72 hpi (Fig. 3*F*). To confirm the ability of SARS-CoV-2 to infect human astrocytes, we used a replication-competent eGFP reporter–pseudotyped vesicular stomatitis virus (VSV) in which the glycoprotein gene (G) of VSV was replaced by the full-length SARS-CoV-2 spike (S; VSV-eGFP-SARS-CoV-2) (36). The human astrocyte culture was also infected by VSV-eGFP-SARS-CoV-2 (Fig. 3 *G* and *H*). Altogether, these results provide strong evidence that human astrocytes are permissive to SARS-CoV-2 infection and also represent a site for viral replication in the CNS.

NRP1 Is Required for Infection of Astrocytes by SARS-CoV-2. Since astrocytes are susceptible to SARS-CoV-2 infection, we searched for the receptor permitting viral entry. To do so, we

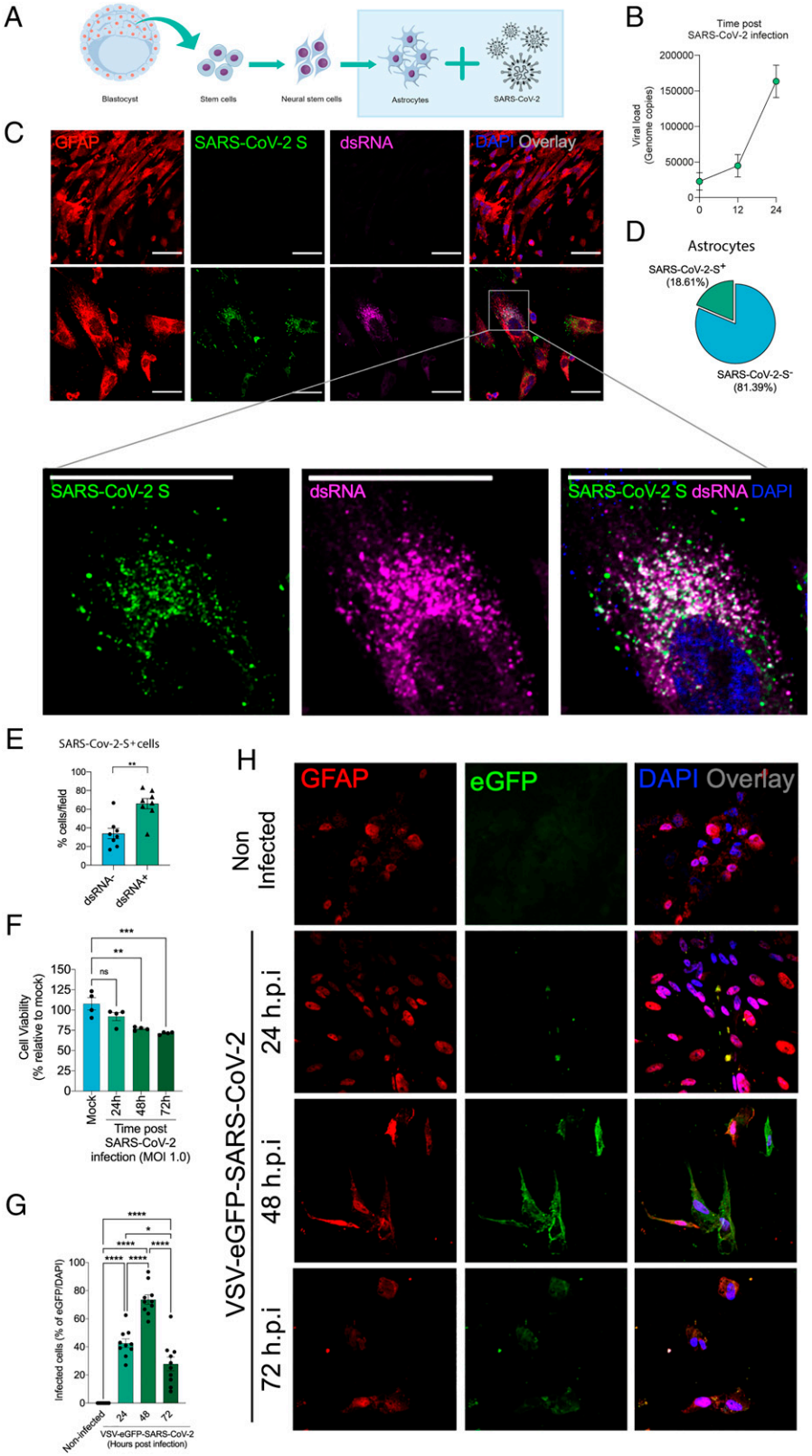

Fig. 3. SARS-CoV-2 infects and replicates in astrocytes in vitro. (*A*) Human neural stem cell–derived astrocytes were infected in vitro with SARS-CoV-2 (MOI 1.0) for 1 h, washed, and harvested 24 h after infection. (*B*) SARS-CoV-2 viral load detection in astrocyte cell pellets ($n = 6$ replicates) using RT-PCR. (*C*) Immunostaining for GFAP (red), ds RNA (magenta), SARS-CoV-2-S (green), and nuclei (DAPI; blue). Images were acquired at 630× magnification. (Scale bars: 50 μm.) (*D*) Percentage of infected astrocytes. The data depict SARS-CoV-2-S and DAPI-stained cells (100 fields were analyzed). (*E*) Frequency of cells containing replicating viruses. (*F*) Astrocyte viability upon SARS-CoV-2 infection was assessed using a luminescence-based cell viability assay (CellTiter-Glo), determining the number of live cells by quantification of ATP at 24, 48, and 72 hpi. (*G*) Percentage of infected cells with pseudotyped SARS-CoV-2 (VSV-eGFP-SARS-CoV-2) at 24, 48, and 72 hpi. (*H*) Staining for DAPI (nuclei; blue), GFAP (astrocytes; red), and eGFP (virus; green) in astrocytes infected with pseudotyped SARS-CoV-2 (VSV-eGFP-SARS-CoV-2) at 24, 48, and 72 hpi. The data represent the percentage of dsRNA-stained cells of SARS-CoV-2-S–positive cells (10 fields were analyzed). All data are representative of at least two independent experiments performed in triplicate or quadruplicate and shown as mean ± SEM. *P* values were determined by two-tailed unpaired tests with Welch's correction (*E*) or one-way ANOVA followed by Tukey's post hoc test (*F* and *G*). *indicate statistical significance. $^{**}P < 0.01$ compared with the mock group; $^{***}P < 0.001$ compared with the mock group; $^{****}P < 0.0001$ compared with the mock group. ATP: adenosine triphosphate; MOI: multiplicity of infection; ns: not significant; DAPI: 4′,6-diamidino-2-phenylindole.

started by using a publicly available, single-nucleus RNA-sequencing (snRNA-seq) dataset from brain samples of patients with COVID-19 (37) to analyze the mRNA expression of the classical SARS-CoV-2 receptor ACE2 as well as the alternative receptors NRP1 and BSG (38–40). These analyses revealed that *ACE2* mRNA was undetected in astrocytes (21, 37); however, astrocytes did express detectable levels of *NRP1* and *BSG* mRNA (Fig. 4 *A* and *B*). We also found that the levels of expression and percentage of astrocytes expressing *NRP1* and *BSG* mRNA were increased in astrocytes from COVID-19 patients compared with controls (Fig. 4 *A* and *B*). Since the binding of SARS-CoV-2 spike to BSG remains controversial (41), we decided to explore the possible role of NRP1. First, we performed western blotting using cultured neural stem cell–derived astrocyte extracts to evaluate if the data from snRNA-seq matched proteome-level data from our in vitro model with ACE2-transduced A549 cells as the positive control. The human astrocytes used in this study did not express ACE2, whereas they did express NRP1 (Fig. 4 *C–E* and *SI Appendix*, Fig. S7).

To determine whether NRP1 was the receptor permitting SARS-CoV-2 infection in astrocytes, we preincubated these cells with a neutralizing anti-NRP1 antibody. Neutralization of NRP1 inhibited the infection of cultured astrocytes by SARS-CoV-2 (Fig. 4*D*) as well as the infection of cultured astrocytes by VSV-eGFP-SARS-CoV-2 (Fig. 4 *E* and *F*). These results confirm that SARS-CoV-2 infects human astrocytes via the NRP1 receptor.

Proteomic and Metabolomic Changes in SARS-CoV-2–Infected Human Astrocytes. To identify pathways triggered by SARS-CoV-2 infection and as such, possibly involved in the changes observed in the brain tissues of COVID-19 patients, we analyzed the proteome of SARS-CoV-2–infected human astrocytes. LC/MS-based shotgun proteomics revealed 170 differentially expressed proteins in SARS-CoV-2–infected astrocytes compared with mock controls, 68 being up-regulated and 102 down-regulated (*SI Appendix*, Fig. S8*A*)—a subset of which was sufficient to compose a molecular signature to clearly distinguish infected astrocytes from mock controls (*SI Appendix*, Fig. S8*B*).

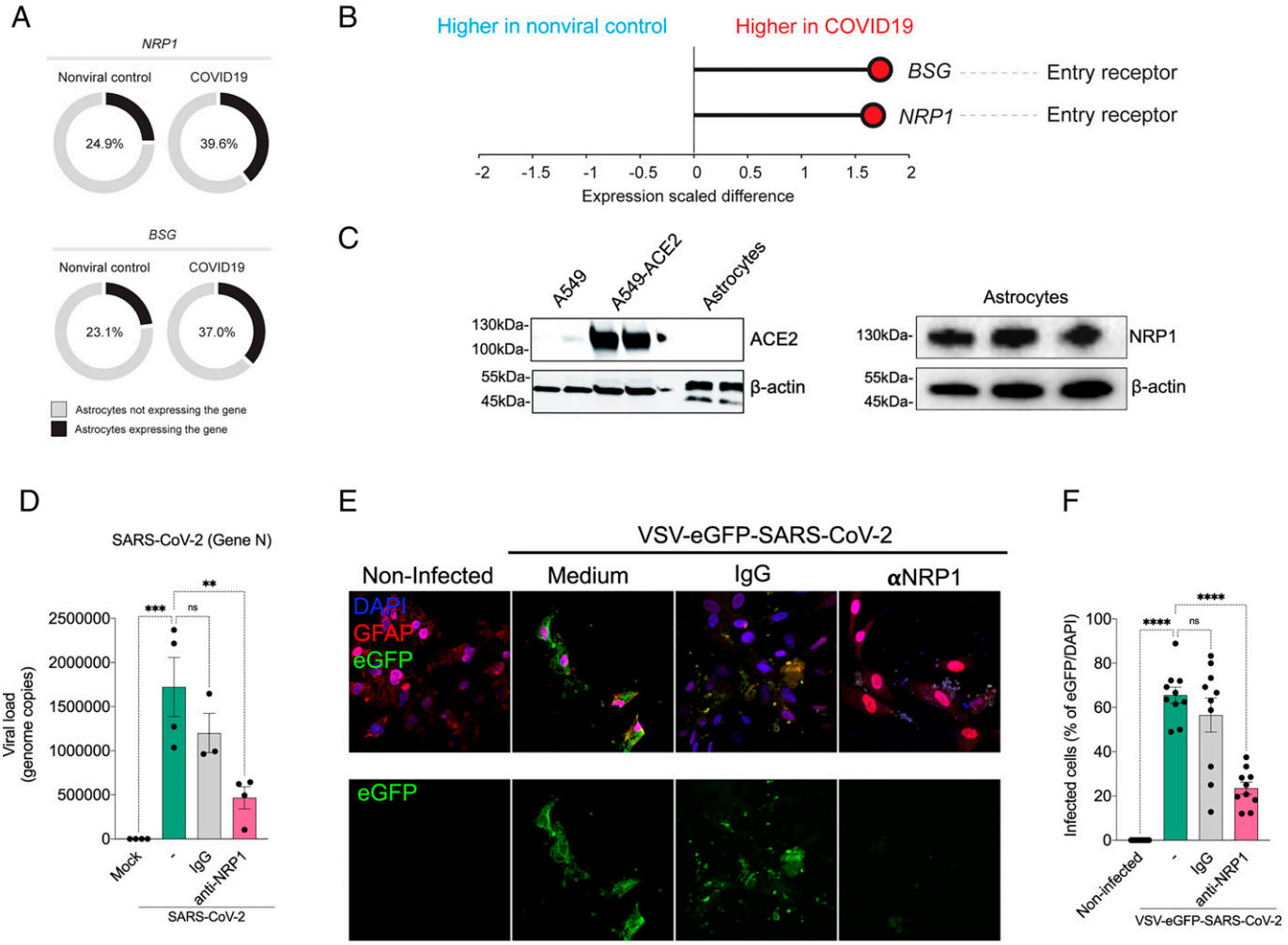

Fig. 4. SARS-CoV-2 infects astrocytes via NRP1. (*A*) Percentage of astrocytes expressing entry receptor genes in COVID-19 patients compared with astrocytes from noninfected controls. (*B*) BSG and NRP1 are differentially expressed in astrocytes from COVID-19 patients compared with astrocytes from noninfected controls. The *x* axis shows the average expression difference (scaled) between COVID-19 patients and noninfected controls. (*C*) Immunoblot analyses of ACE2 and NRP1 using an extract of noninfected neural stem cell–derived astrocytes. Beta-actin was used as the loading control. To control for ACE2 expression, we used A549 cells and A549 cells overexpressing ACE2. (*D*) Neural stem cell–derived astrocytes were preincubated with an NRP1-neutralizing antibody and then harvested 24 hpi to measure the SARS-CoV-2 viral load. (*E*) Astrocytes were stained for DAPI (nuclei; blue), GFAP (astrocytes; red), and eGFP (virus; green). Cells were preincubated with the NRP1-neutralizing antibody and then assessed 48 hpi with the SARS-CoV-2 pseudotyped virus (VSV-eGFP-SARS-CoV-2). (Scale bars: 50 μm.) (*F*) Percentage of infected cells. Images were acquired at 630× magnification. All data are representative of at least two independent experiments performed in triplicate and shown as mean ± SEM. *P* values were determined by one-way ANOVA followed by Tukey's post hoc test (*D* and *F*). $^{**}P < 0.01$ compared with the mock group; $^{***}P < 0.001$ compared with the mock group; $^{****}P < 0.0001$ compared with the mock group. DAPI: 4′,6-diamidino-2-phenylindole; ns: non significant.

Using these altered proteins, pathway enrichment and interactome analyses predicted a wide range of biological processes and regulatory networks affected by SARS-CoV-2 infection (Fig. 5*A*). Pathways involved in carbon/glucose metabolism were among the most enriched (Fig. 5*B*). More specifically, proteins found differentially expressed in SARS-CoV-2–infected astrocytes and in COVID-19 postmortem brain tissue samples belonged to glycolysis/gluconeogenesis, carbon metabolism, and the pentose phosphate pathway (Fig. 5*C*). Collectively, these data reinforce that SARS-CoV-2 infects astrocytes in the CNS, possibly affecting energy metabolism pathways and modulating proteins associated with neurodegeneration.

Since there are significant proteomic alterations in metabolic pathways, we sought to investigate if the infection of human astrocytes impacts the levels of key metabolites involved in energy metabolism. LC/MS-based metabolomic analysis of SARS-CoV-2–infected astrocytes showed pronounced changes in metabolic intermediates of glycolysis and anaplerotic reactions, indicating alterations in the pathways of astrocyte metabolism (*SI Appendix*, Fig. S9*A*). This phenomenon was marked by a decrease in pyruvate and lactate, which are downstream metabolites of the glycolytic pathway, as well as a reduction in glutamine and intermediates of glutamine metabolism, such as glutamate, GABA, and alpha-ketoglutarate (*SI Appendix*, Fig. S9*A*). Despite these alterations, there were no significant changes in tricarboxylic acid cycle (TCA cycle) intermediates (*SI Appendix*, Fig. S9*B*). Considering the reduction of lactate levels in SARS-CoV-2–infected astrocytes, we evaluated the expression of monocarboxylate transporter (MCT); both *MCT1* and *MCT2* levels were reduced in SARS-CoV-2–infected astrocytes when compared with the mock control (*SI Appendix*, Fig. S9*C*). SARS-CoV-2–infected astrocyte bioenergetics were further characterized by Seahorse Extracellular Flux analysis, showing increased

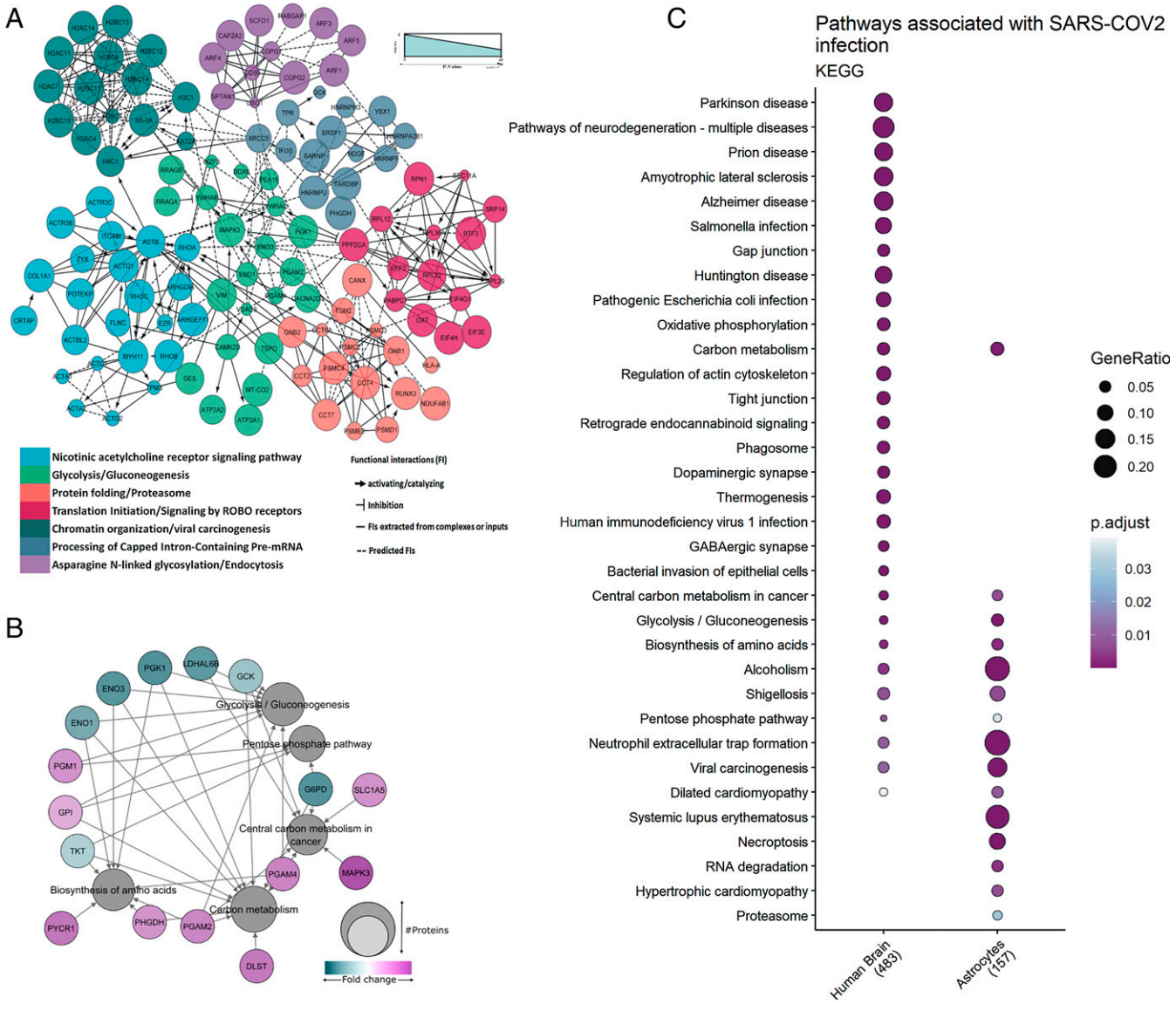

Fig. 5. Proteomic changes in SARS-CoV-2–infected human astrocytes and postmortem brain tissue from COVID-19 patients. (*A*) Reactome functional interaction network of differentially regulated genes in human neural stem cell–derived astrocytes infected with SARS-CoV-2. Seven protein clusters as indicated by the color of enriched pathways; the line types represent protein–protein interactions and downstream activation or inhibition related to gene modulation, showing how some pathways can be affected by SARS-CoV-2 infection ($P < 0.05$ calculated based on binomial test). (*B*) Network of proteins found differentially regulated in SARS-COV-2–infected astrocytes and their respective pathways, enriched according to the KEGG (Kyoto Encyclopedia of Genes and Genomes) database. The pathways are represented by gray circles, and their size is proportional to the number of proteins differentially regulated; proteins are represented by the colored circles, which are colored according to their fold change. (*C*) KEGG enrichment analysis of differentially expressed proteins in SARS-CoV-2–infected astrocytes vs. mock as compared with postmortem brain tissue from COVID-19 patients vs. controls. Dot size represents the number of proteins related to the respective cell type, and the color represents the *P* value adjusted by false discovery rate. ROBO: Roundabout protein family.

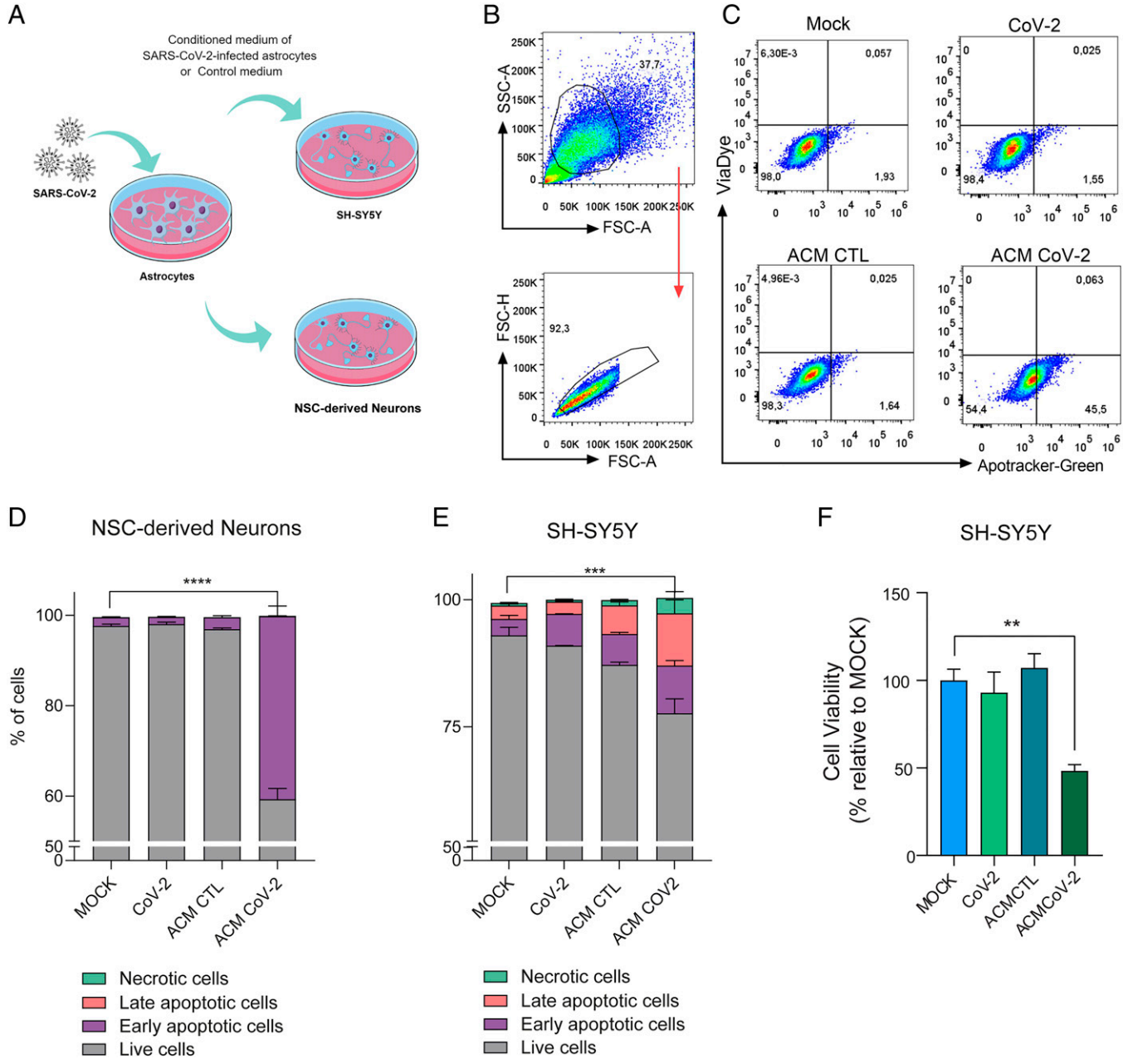

Fig. 6. Medium conditioned by SARS-CoV-2–infected astrocytes reduces neuronal viability. (*A*) Human NSC-derived neurons and SH-SY5Y neuronal cells were cultured for 24 h in the presence of medium conditioned by uninfected astrocytes (mock infection; ACM CTL) or SARS-CoV-2–infected astrocytes (ACM CoV-2). (*B*) Cellular viability as measured by apotracker/fixable viability stain (FVS) and analyzed by flow cytometry. Representative gating strategies are shown. (*C*) Representative dot plots of neuronal viability. Percentage of living or nonliving (*D*) NSC-derived neurons and (*E*) SH-SY5Y cells. Cells were classified as living (gray bars; double negative), in early apoptosis (purple bars; apotracker+/FVS−), in late apoptosis (pink bars; double positive), or necrotic (green bars; apotracker−/FVS+). (*F*) Differentiated SH-SY5Y cells were cultured for 24 h in the presence of medium conditioned by SARS-CoV-2–infected astrocytes (ACM CoV-2) or uninfected astrocytes (ACM CTL). The viability of SH-SY5Y cells was assessed using an ATP (adenosine triphosphate) -quantifying, luminescence-based cell viability assay (CellTiter-Glo) at 24 h postinfection. *P* values were determined by one-way ANOVA followed by Tukey's post hoc test. $^{**}P < 0.01$ compared with the mock group; $^{***}P < 0.001$ compared with the mock group; $^{****}P < 0.0001$ compared with the mock group. ATP: adenosine triphosphate; SSC-A: Side scatter area; FSC-H: Forward scatter height; FSC-A: Forward scatter area.

respiration in infected cells (*SI Appendix*, Fig. S9*D*). This was due to an increase in both mitochondrial (maximal respiration) and nonmitochondrial oxygen consumption; the former was linked to higher proton leak, indicating increased uncoupled respiration (*SI Appendix*, Fig. S9 *D* and *E*). Together, these results demonstrate increased oxidative metabolism in SARS-CoV-2–infected astrocytes and a reduction of the levels of metabolites produced by these cells to support neuronal metabolism and function (*SI Appendix*, Fig. S9*F*).

Conditioned Medium from SARS-CoV-2–Infected Astrocytes Reduces Neuronal Viability. Astrocytes are essential to brain homeostasis not only because they are the main energy reservoirs of the brain (42) but also, due to their important role in protective responses to cell damage triggered by infection or sterile inflammation (43, 44). There is evidence that astrocytes may secrete yet undetermined neurotoxic factors (43–45) and are also involved in the uptake, synthesis, and distribution of brain metabolites (46, 47). Thus, we investigated if neuronal viability could be affected by exposure to media conditioned by SARS-CoV-2–infected astrocytes. To test this hypothesis, we cultured NSC-derived neurons or differentiated SH-SY5Y neurons for 24 h in a control or conditioned medium in which SARS-CoV-2–infected astrocytes were grown (Fig. 6*A*). The conditioned medium increased the rates of apoptosis by 45.5 and

22.7% in NSC-derived neurons and SH-SY5Y neurons, respectively (Fig. 6 *B*–*E* and *SI Appendix*, Fig. S10 *A* and *B*). The possibility of neuronal infection was ruled out as viral RNA was not detected in either cell type after exposure to the conditioned medium (*SI Appendix*, Fig. S10 *E* and *F*), and direct exposure to SARS-CoV-2 did not reduce the viability of NSC-derived neurons or SH-SY5Y neurons after 24 (Fig. 6 *D* and *E*), 48, or 72 h (*SI Appendix*, Fig. S10 *C* and *D*). These results suggest that SARS-CoV-2–infected astrocytes release soluble factors, which reduce neuronal viability.

Discussion

Our study demonstrates structural and functional alterations in the brain tissue of COVID-19 patients, which parallel in vivo findings of cortical atrophy, neuropsychiatric symptoms, and cognitive dysfunctions. A recent longitudinal study with 401 individuals (median age of 62 y, infected between March 2020 and April 2021, scanned pre- and postinfection) reported atrophy in the orbitofrontal and parahippocampal regions and cognitive impairment (determined by Color Trail tests) (48). The patients we analyzed were infected between March and July 2020 (and therefore, were most likely infected with the original SARS-CoV-2 strain), and we also observed atrophy in the orbitofrontal area and cognitive dysfunction (longer time to perform Color Trail tests and poorer verbal memory task performance). Interestingly, patients with only mild COVID-19 also exhibited cortical atrophy in the superior temporal gyrus, which was previously described in a group of patients with severe SARS-CoV-2 infection (49). We also observed that higher levels of anxiety symptoms correlated with atrophy of the orbitofrontal cortex, a region previously linked with anxiety disorders (50). Our results suggest that anxiety and depression symptoms are at least partially associated with SARS-CoV-2 infection, a hypothesis supported by a recently discovered association between anxiety and reactive astrogliosis in patients after COVID-19 (51).

This study and other reports showing alterations in brain structure and the manifestation of neurological symptoms in COVID-19 patients (52–54) raise a debate on whether these clinical features are a consequence of peripheral changes or rather, viral invasion of the CNS. Both hypotheses are possible as we detected histopathological alterations associated with SARS-CoV-2 presence in brain tissue collected from 5 deceased patients, while 21 individuals who died of COVID-19 did not show any brain tissue alterations. However, as the sampling region was small, the possibility remains that other brain regions may exhibit COVID-19–related histopathological alterations. Indeed, the limited number of individuals who exhibited brain alterations associated with CNS SARS-CoV-2 detection and the imprecise and heterogenic nature of postmortem sample collection across studies may explain the discussion regarding the potential correlations between neuroinvasion and COVID-19 symptoms (22, 25–27, 55, 56). Although some studies failed to detect the virus in the CNS (57), others have found viral particles in the brain (21) localized to the microvasculature and neurons (22), the choroid plexus (58), or meninges (59). In vitro models, such as stem cell–derived neural cells and cerebral organoids, have also demonstrated that SARS-CoV-2 potentially infects brain cells (22, 25–27, 55). However, the magnitude of the CNS infection, its distribution within the brain tissue, and the molecular and cellular bases underlying the phenomenon had not been thoroughly explored. Here, we show that astrocytes are the main site of infection—and possibly, replication—of SARS-CoV-2 in the brains of COVID-19 patients as evidenced by the detection of the viral genome, the SARS-CoV-2 spike protein, and dsRNA in postmortem brain tissue, ex vivo brain slices, and in vitro infected astrocytes. These findings corroborate other studies that showed that astrocytes from primary human cortical tissue and stem cell–derived cortical organoids are susceptible to SARS-CoV-2 infection (22, 55, 60).

Recently, Meinhardt et al. (61) described that SARS-CoV-2 could access the CNS through the neural–mucosal interface in olfactory mucosa, thereby entering the primary respiratory and cardiovascular control centers in the medulla oblongata. Other proposed routes of SARS-CoV-2 neuroinvasion include brain endothelial cells (28–30, 32, 61, 62). In addition to the inflammatory response produced by SARS-CoV-2 infection, endothelial cell infection could also cause dysfunctions in BBB integrity and facilitate further access of the virus to the brain (28–30, 32, 61, 62). Despite the advances that have already been made, there is still much left to be learned about the routes that SARS-CoV-2 can take to invade the brain and how the virus navigates across different brain regions.

While ACE2 is the best-characterized cellular receptor for SARS-CoV-2 to enter cells via interaction with the viral spike protein, other receptors have also been identified as mediators of infection (63). According to our data and others (21), astrocytes do not express ACE2; rather, they exhibit elevated expression of NRP1, another SARS-CoV-2 spike target that is abundantly expressed in the CNS, particularly in astrocytes (Fig. 5*C*) (38, 39, 64). When NRP1 is blocked with neutralizing antibodies, SARS-CoV-2 infection in these cells is greatly reduced. These results indicate that SARS-CoV-2 infects in vitro astrocytes via the NRP1 receptor, although this has yet to be confirmed in vivo.

To understand the consequences of SARS-CoV-2 infection in NSC-derived astrocytes, we searched for changes in the proteome in a nonhypothesis-driven fashion. SARS-CoV-2 infection resulted in marked proteomic changes in several biological processes, including those associated with energy metabolism, in line with previous reports on other cell types infected with SARS-CoV-2 (65–67). Noteworthily, differentially expressed proteins in COVID-19 postmortem brains were enriched for astrocytic proteins more than oligodendrocytes, neurons, or Schwann cells, strengthening our findings that these are the most affected cells by SARS-CoV-2 infection in the human brain. Our proteomic data also evidenced changes in the components of carbon metabolism pathways, particularly glucose metabolism, in both in vitro infected astrocytes and postmortem brain tissue from COVID-19 patients.

Since astrocyte metabolism is key to support neuronal function, changes in astrocyte metabolism could indirectly impact neurons. We found that one of the most critical alterations caused by SARS-CoV-2 infection in astrocytes was a decrease in pyruvate and lactate levels. Lactate exportation is one of the ways that astrocytes support neurons metabolically (63), shuttling this carbon source through the astrocyte–neuron lactate shuttle (ANLS) mechanism. In the ANLS, neuronal activity also enhances glutamate uptake by astrocytes (68). Lactate itself is essential for the support of neuronal activity and cerebral functions, acting as a neuroprotective agent as well as a key signal to regulate blood flow (69). These metabolic changes, particularly the reductions in lactate and pyruvate associated with decreases in *MCT1* and *MCT2* expression in SARS-CoV-2–infected astrocytes, support the hypothesis of ANLS disruption. Moreover, intermediates of glutamine metabolism, such as glutamate and GABA, were also decreased in SARS-CoV-2–infected astrocytes. This said, there were no significant changes in any core intermediates of the TCA

cycle. Together with an increased oxygen consumption rate of SARS-CoV-2–infected astrocytes, these results suggest that glycolysis and glutaminolysis are being used to fuel carbons into the TCA cycle to sustain the increased oxidative metabolism of infected astrocytes. Recently, de Oliveira et al. (24) showed that glutamine levels were also found reduced in mixed glial cells infected with SARS-CoV-2 and that the inhibition of glutaminolysis decreased viral replication and proinflammatory response, further reinforcing that glutamine could be used to fuel the TCA cycle in infected astrocytes.

While astrocyte-derived lactate is required for neuronal metabolism (47, 70), as previously mentioned, glutamine is used in the synthesis of neurotransmitters, such as glutamate and GABA (71). Astrocytes also play a vital role in glutamate-level homeostasis (72, 73) and neurotransmitter recycling, crucial processes for the maintenance of synaptic transmission and neuronal excitability. At glutamatergic synapses, glutamate uptake by astroglia prevents excitotoxicity (74), whereupon glutamine synthetase converts glutamate to glutamine, which can then be transferred back to neurons, thus closing the glutamate–glutamine cycle (75). At GABAergic synapses, GABA is taken up by astrocytes and first metabolized to glutamate before being converted to glutamine (76). Given the importance of the metabolic coupling between astrocytes and neurons, alterations in astrocytic glucose and glutamine metabolism are expected to compromise neuronal metabolism and plasticity and synaptic function (77). By 18F-FDG PET analysis, Guedj et al. (78) reported hypometabolism in four different clusters of brain regions in patients suffering from long COVID-19, including the bilateral rectal/orbital gyrus and the olfactory gyrus (78). As key regulators of CNS metabolism, alterations in astrocyte metabolism contribute to the 18F-FDG PET signal (79–81). Therefore, dysfunctions in astrocyte energy metabolism, like those observed here, could explain, at least partially, the brain hypometabolism in COVID-19 patients (78, 82–85).

In addition to the metabolic changes observed in SARS-CoV-2–infected astrocytes that may lead to neuronal dysfunction, we found that SARS-CoV-2 infection elicits a neurotoxic secretory phenotype in astrocytes that results in increased neuronal death. A similar phenomenon has been observed when astrocytes are activated by inflammatory factors (43, 86, 87). The alterations in cortical thickness we observed in COVID-19 patients could be explained by this neuronal death, at least partially, as well as by other mechanisms, including reactive astrogliosis and alterations in astrocyte specification and morphogenesis, as previously described in Alzheimer's disease, autism, and schizophrenia (88–90), as well as epilepsy, autism, and self-injury (91–94). Matschke et al. (21) reported astrogliosis in 86% of individuals who died following a diagnosis of SARS-CoV-2 infection. In agreement, snRNA-seq data show that the main markers of reactive astrocytes (95) are enriched in samples from the medial frontal cortex of patients with COVID-19 compared with noninfected patients, supporting the hypothesis that reactive astrogliosis is a feature of COVID-19 (*SI Appendix*, Fig. S11). Astrocytes are also relevant in the regulation of synapses (and neural networks) and have been linked to the manifestation of depression (96), anxiety symptoms (97), and memory impairment (98), all of which have been observed in our post-COVID infection cohort.

In summary, our findings are consistent with a model in which SARS-CoV-2 is able to reach the CNS of COVID-19 patients, infect astrocytes via NRP1 interaction, and secondarily impair neuronal function and viability. These changes may contribute to the alterations of brain structure observed here and elsewhere, thereby resulting in the neurocognitive and neuropsychiatric dysfunctions manifested by some patients with COVID-19. Our study comes as a cautionary note that mechanisms of neuroinvasion in fatal COVID-19 could also be operative in mild COVID-19. However, it is important to note that the study was limited in that neuroimaging and cognitive testing were obtained from a different cohort than fatal COVID-19, in which only a minority of individuals showed evidence of astrocytic invasion. Nonetheless, interventions directed to treat COVID-19 should also envision ways to prevent SARS-CoV-2 invasion of the CNS and/or replication in astrocytes.

Materials and Methods

The neuropsychological evaluations and neuroimaging analyses were approved by the Research Ethics Committee of the University of Campinas (CAAE no. 31556920.0.0000.5404), and all subjects signed a consent form to participate. The autopsy studies were approved by the National Commission for Research Ethics (CAAE nos. 32475220.5.0000.5440 and 38071420.0.1001.5404). Full details involving the brain imaging and neuropsychological evaluation; postmortem brain samples from COVID-19; human brain slice cultures; generation of human astrocytes (hES derived); in vitro infection; metabolomic, proteomic, gene expression, viral load, flow cytometry, and bioenergetics assays; and immunostaining details are provided in *SI Appendix, Materials and Methods*.

Data, Materials, and Software Availability. Mass spectrometry proteomic data have been deposited in the ProteomeXchange Consortium via the PRIDE (43) partner repository (accession no. PXD023781) (99). All other data are included in the article and/or SI Appendix.

ACKNOWLEDGMENTS. We thank Edison Durigon for providing the SARS-CoV-2 virus. We thank Gabriela Lopes Vitória, Elzira E. Saviani, and Paulo Baldasso for technical support.

Author affiliations: [a]Department of Biochemistry and Tissue Biology, Institute of Biology, University of Campinas, Campinas, 13083862, Brazil; [b]Ribeirão Preto Medical School, University of São Paulo, Ribeirão Preto, 14049900, Brazil; [c]University of São Paulo, São Paulo, 05508-220, Brazil; [d]D'Or Institute for Research and Education, 04502001, Brazil; and [e]Institute of Biomedical Science, Federal University of Rio de Janeiro, Rio de Janeiro, 21941590, Brazil

Author contributions: F. Crunfli, V.C.C., F.P.V., L.S.S., M.H.N., A.S.L.M.A., A.G.F.V., C.B.-T., G.d.S.Z., A.C.C., G.F.d.S., S.P.M., P.L.P., Í.M.S.d.C., G.M.A., I.M.P., B.M.S.S., R.M.G., N.D.M., G.G.D., J.A.G., M.N.B., S.S.B., L.S., R.B.J., Í.K.A., M.R.d.B., M.J.M., B.A.d.C., M.K.M.A., J.R.d.S.J., L.L.D., I.M.P.d.S., E.D.d.R., S.M.G., L.H.L.d.S., V.B., B.M.C., G.L., M.C.P., R.M.M.V., R.B.M., A.S.V., J.C.A.-F., E.A., G.G.P.-G., M.V.S., L.N., A.D., S.R., M.A.R.V., C.D.M., P.L.-J., R.D.O., F.Q.C., H.I.N., T.M., A.N.D.-N., L.F.F.d.S., M.D., P.H.N.S., A.S.F., F. Cendes, P.M.M.M.-V., A.T.F., A.S., J.L.P.-M., C.L.Y., M.A.M., T.M.C., and D.M.-d.-S. designed research; F. Crunfli, V.C.C., F.P.V., L.S.S., M.H.N., A.S.L.M.A., P.H.V., A.G.F.V., C.B.-T., G.d.S.Z., V.M.S.-C., A.C.C., G.F.d.S., S.P.M., P.L.P., D.A.T.-T., B.M.M., G.M.A., E.M.S.F., I.M.P., B.M.S.S., R.M.G., N.D.M., R.G.L., G.P.R., T.L.K., G.G.D., J.A.G., P.B.R., J.F., M.R.A., N.B.S., M.N.B., S.S.B., L.S., R.B.J., Í.K.A., M.R.d.b., M.J.M., B.A.d.C., M.K.M.A., J.R.d.S.J., L.L.D., I.M.P.d.S., E.D.d.R., S.M.G., L.H.L.d.S., V.B., B.M.C., L.A.T., M.C.P., R.M.M.V., R.B.M., G.G.P.-G., M.V.S., L.N., C.D.M., T.M., A.N.D.-N., L.F.F.d.S., M.D., P.H.N.S., F. Cendes, A.S., and C.L.Y. performed research; M.C.M., A.S.V., J.C.A.-F., E.A., S.R., M.A.R.V., C.D.M., P.L.-J., R.D.O., F.Q.C., M.D., P.H.N.S., A.T.F., and J.L.P.-M. contributed new reagents/analytic tools; F. Crunfli, V.C.C., F.P.V., L.S.S., M.H.N., A.S.L.M.A., P.H.V., G.R.-d.-O., L.C.S.-C., V.M.S.-C., B.J.S., A.C.C., Í.M.S.d.C., G.M.A., B.M.S.S., S.S.B., L.S., G.L., E.A., G.G.P.-G., M.V.S., L.N., H.I.N., F. Cendes, P.M.M.M.-V., A.T.F., A.S., J.L.P.-M., C.L.Y., M.A.M., T.M.C., and D.M.-d.-S. analyzed data; and F. Crunfli, V.C.C., F.P.V., L.S.S., M.H.N., B.M.S.S., B.M.C., G.L., F.C., P.M.M.M.-V., A.T.F., A.S., J.L.P.-M., C.L.Y., M.A.M., T.M.C., and D.M.-d.-S. wrote the paper.

The authors declare no competing interest.

[1]F. Crunfli, V.C.C., and F.P.V. contributed equally to this work.

[2]To whom correspondence may be addressed. Email: cyasuda@unicamp.br, morima@unicamp.br, thicunha@fmrp.usp.br, or dmsouza@unicamp.br.

This article contains supporting information online at http://www.pnas.org/lookup/suppl/doi:10.1073/pnas.2200960119/-/DCSupplemental.

1. X. Yang *et al.*, Clinical course and outcomes of critically ill patients with SARS-CoV-2 pneumonia in Wuhan, China: A single-centered, retrospective, observational study. *Lancet Respir. Med.* **8**, 475–481 (2020).
2. A. Gupta *et al.*, Extrapulmonary manifestations of COVID-19. *Nat. Med.* **26**, 1017–1032 (2020).
3. A. Nalbandian *et al.*, Post-acute COVID-19 syndrome. *Nat. Med.* **27**, 601–615 (2021).
4. K. Kotfis *et al.*, COVID-19: ICU delirium management during SARS-CoV-2 pandemic. *Crit. Care* **24**, 176 (2020).
5. L. Mao *et al.*, Neurologic manifestations of hospitalized patients with coronavirus disease 2019 in Wuhan, China. *JAMA Neurol.* **77**, 683–690 (2020).

6. A. Varatharaj *et al.*; CoroNerve Study Group, Neurological and neuropsychiatric complications of COVID-19 in 153 patients: A UK-wide surveillance study. *Lancet Psychiatry* **7**, 875–882 (2020).
7. Y. Lu *et al.*, Cerebral micro-structural changes in COVID-19 patients - An MRI-based 3-month follow-up study. *EClinicalMedicine* **25**, 100484 (2020).
8. F. Zhou *et al.*, Clinical course and risk factors for mortality of adult inpatients with COVID-19 in Wuhan, China: A retrospective cohort study. *Lancet* **395**, 1054–1062 (2020).
9. G. D. Batty *et al.*, Psychosocial factors and hospitalisations for COVID-19: Prospective cohort study based on a community sample. *Brain Behav. Immun.* **89**, 569–578 (2020).
10. B. C. Mcloughlin *et al.*, Functional and cognitive outcomes after COVID-19 delirium. *Eur. Geriatr. Med.* **11**, 857–862 (2020).
11. P. Pinna *et al.*, Neurological manifestations and COVID-19: Experiences from a tertiary care center at the Frontline. *J. Neurol. Sci.* **415**, 116969 (2020).
12. F. G. De Felice, F. Tovar-Moll, J. Moll, D. P. Munoz, S. T. Ferreira, Severe acute respiratory syndrome coronavirus 2 (SARS-CoV-2) and the central nervous system. *Trends Neurosci.* **43**, 355–357 (2020).
13. J. Xu *et al.*, Detection of severe acute respiratory syndrome coronavirus in the brain: Potential role of the chemokine mig in pathogenesis. *Clin. Infect. Dis.* **41**, 1089–1096 (2005).
14. K.-K. Lau *et al.*, Possible central nervous system infection by SARS coronavirus. *Emerg. Infect. Dis.* **10**, 342–344 (2004).
15. E. C. W. Hung *et al.*, Detection of SARS coronavirus RNA in the cerebrospinal fluid of a patient with severe acute respiratory syndrome. *Clin. Chem.* **49**, 2108–2109 (2003).
16. T. Moriguchi *et al.*, A first case of meningitis/encephalitis associated with SARS-Coronavirus-2. *Int. J. Infect. Dis.* **94**, 55–58 (2020).
17. Y. H. Huang, D. Jiang, J. T. Huang, SARS-CoV-2 detected in cerebrospinal fluid by PCR in a case of COVID-19 encephalitis. *Brain Behav. Immun.* **87**, 149 (2020).
18. R. Bernard-Valnet *et al.*, Two patients with acute meningoencephalitis concomitant with SARS-CoV-2 infection. *Eur. J. Neurol.* **27**, e43–e44 (2020).
19. L. S. Politi, E. Salsano, M. Grimaldi, Magnetic resonance imaging alteration of the brain in a patient with coronavirus disease 2019 (COVID-19) and anosmia. *JAMA Neurol.* **77**, 1028–1029 (2020).
20. R. R. Reichard *et al.*, Neuropathology of COVID-19: A spectrum of vascular and acute disseminated encephalomyelitis (ADEM)-like pathology. *Acta Neuropathol.* **140**, 1–6 (2020).
21. J. Matschke *et al.*, Neuropathology of patients with COVID-19 in Germany: A post-mortem case series. *Lancet Neurol.* **19**, 919–929 (2020).
22. E. Song *et al.*, Neuroinvasion of SARS-CoV-2 in human and mouse brain. bioRxiv [Preprint] (2020). https://www.biorxiv.org/content/10.1101/2020.06.25.169946v2 (Accessed 8 November 2020).
23. F. S. Oladunni *et al.*, Lethality of SARS-CoV-2 infection in K18 human angiotensin-converting enzyme 2 transgenic mice. *Nat. Commun.* **11**, 6122 (2020).
24. L. G. de Oliveira *et al.*, SARS-CoV-2 infection impacts carbon metabolism and depends on glutamine for replication in Syrian hamster astrocytes. bioRxiv [Preprint] (2021). https://www.biorxiv.org/content/10.1101/2021.10.23.465567v1 (Accessed 30 October 2021).
25. A. Ramani *et al.*, SARS-CoV-2 targets neurons of 3D human brain organoids. *EMBO J.* **39**, e106230 (2020).
26. B.-Z. Zhang *et al.*, SARS-CoV-2 infects human neural progenitor cells and brain organoids. *Cell Res.* **30**, 928–931 (2020).
27. J. Zheng *et al.*, COVID-19 treatments and pathogenesis including anosmia in K18-hACE2 mice. *Nature* **589**, 603–607 (2021).
28. L. Zhang *et al.*, SARS-CoV-2 crosses the blood-brain barrier accompanied with basement membrane disruption without tight junctions alteration. *Signal Transduct. Target. Ther.* **6**, 337 (2021).
29. A. Grieco, *Long Covid: Una nuova sfida oltre l'emergenza. Come ritrovarebenessere e salute dopo il Covid-19* (Naturvis Books, 2021).
30. L. Pellegrini *et al.*, SARS-CoV-2 infects the brain choroid plexus and disrupts the blood-CSF barrier in human brain organoids. *Cell Stem Cell* **27**, 951–961.e5 (2020).
31. T. P. Buzhdygan *et al.*, The SARS-CoV-2 spike protein alters barrier function in 2D static and 3D microfluidic in-vitro models of the human blood-brain barrier. *Neurobiol. Dis.* **146**, 105131 (2020).
32. J. L. Reynolds, S. D. Mahajan, SARS-COV2 alters blood brain barrier integrity contributing to neuro-inflammation. *J. Neuroimmune Pharmacol.* **16**, 4–6 (2021).
33. B. Li *et al.*, Prevalence and impact of cardiovascular metabolic diseases on COVID-19 in China. *Clin. Res. Cardiol.* **109**, 531–538 (2020).
34. F. Weber, V. Wagner, S. B. Rasmussen, R. Hartmann, S. R. Paludan, Double-stranded RNA is produced by positive-strand RNA viruses and DNA viruses but not in detectable amounts by negative-strand RNA viruses. *J. Virol.* **80**, 5059–5064 (2006).
35. A. M. Fraga *et al.*, Establishment of a Brazilian line of human embryonic stem cells in defined medium: Implications for cell therapy in an ethnically diverse population. *Cell Transplant.* **20**, 431–440 (2011).
36. J. B. Case *et al.*, Neutralizing antibody and soluble ACE2 inhibition of a replication-competent VSV-SARS-CoV-2 and a clinical isolate of SARS-CoV-2. *Cell Host Microbe* **28**, 475–485.e5 (2020).
37. A. C. Yang *et al.*, Dysregulation of brain and choroid plexus cell types in severe COVID-19. *Nature* **595**, 565–571 (2021).
38. J. L. Daly *et al.*, Neuropilin-1 is a host factor for SARS-CoV-2 infection. *Science* **370**, 861–865 (2020).
39. L. Cantuti-Castelvetri *et al.*, Neuropilin-1 facilitates SARS-CoV-2 cell entry and infectivity. *Science* **370**, 856–860 (2020).
40. K. Wang *et al.*, CD147-spike protein is a novel route for SARS-CoV-2 infection to host cells. *Signal Transduct. Target Ther.* **5**, 283 (2020).
41. J. Shilts, T. W. M. Crozier, E. J. D. Greenwood, P. J. Lehner, G. J. Wright, No evidence for basigin/CD147 as a direct SARS-CoV-2 spike binding receptor. *Sci. Rep.* **11**, 413 (2021).
42. N. Rouach, A. Koulakoff, V. Abudara, K. Willecke, C. Giaume, Astroglial metabolic networks sustain hippocampal synaptic transmission. *Science* **322**, 1551–1555 (2008).
43. S. A. Liddelow *et al.*, Neurotoxic reactive astrocytes are induced by activated microglia. *Nature* **541**, 481–487 (2017).
44. S. P. Yun *et al.*, Block of A1 astrocyte conversion by microglia is neuroprotective in models of Parkinson's disease. *Nat. Med.* **24**, 931–938 (2018).
45. K. A. Guttenplan *et al.*, Knockout of reactive astrocyte activating factors slows disease progression in an ALS mouse model. *Nat. Commun.* **11**, 3753 (2020).
46. I. A. Simpson, A. Carruthers, S. J. Vannucci, Supply and demand in cerebral energy metabolism: The role of nutrient transporters. *J. Cereb. Blood Flow Metab.* **27**, 1766–1791 (2007).
47. G. K. Gandhi, N. F. Cruz, K. K. Ball, G. A. Dienel, Astrocytes are poised for lactate trafficking and release from activated brain and for supply of glucose to neurons. *J. Neurochem.* **111**, 522–536 (2009).
48. G. Douaud *et al.*, SARS-CoV-2 is associated with changes in brain structure in UK Biobank. *Nature* **604**, 697–707 (2022).
49. Y. Qin *et al.*, Long-term microstructure and cerebral blood flow changes in patients recovered from COVID-19 without neurological manifestations. *J. Clin. Invest.* **131**, e147329 (2021).
50. M. R. Milad, S. L. Rauch, The role of the orbitofrontal cortex in anxiety disorders. *Ann. N. Y. Acad. Sci.* **1121**, 546–561 (2007).
51. B. A. Hanson *et al.*, Plasma biomarkers of neuropathogenesis in hospitalized patients with COVID-19 and those with postacute sequelae of SARS-CoV-2 infection. *Neurol. Neuroimmunol. Neuroinflamm.* **9**, 9 (2022).
52. E. A. Troyer, J. N. Kohn, S. Hong, Are we facing a crashing wave of neuropsychiatric sequelae of COVID-19? Neuropsychiatric symptoms and potential immunologic mechanisms. *Brain Behav. Immun.* **87**, 34–39 (2020).
53. J. P. Rogers *et al.*, Psychiatric and neuropsychiatric presentations associated with severe coronavirus infections: A systematic review and meta-analysis with comparison to the COVID-19 pandemic. *Lancet Psychiatry* **7**, 611–627 (2020).
54. R. Klein *et al.*, COVID-19 induces neuroinflammation and loss of hippocampal neurogenesis. Research Square [Preprint] (2021). https://www.researchsquare.com/article/rs-1031824/v1 (Accessed 5 November 2021).
55. L. Wang *et al.*, A human three-dimensional neural-perivascular 'assembloid' promotes astrocytic development and enables modeling of SARS-CoV-2 neuropathology. *Nat. Med.* **27**, 1600–1606 (2021).
56. A. C. Yang *et al.*, Dysregulation of brain and choroid plexus cell types in severe COVID-19. *Nature* **595**, 565–571 (2021).
57. D. G. Placantonakis *et al.*, SARS-CoV-2 is not detected in the cerebrospinal fluid of encephalopathic COVID-19 patients. *Front. Neurol.* **11**, 587384 (2020).
58. F. Jacob *et al.*, Human pluripotent stem cell-derived neural cells and brain organoids reveal SARS-CoV-2 neurotropism predominates in choroid plexus epithelium. *Cell Stem Cell* **27**, 937–950 (2020).
59. H. Yavarpour-Bali, M. Ghasemi-Kasman, Update on neurological manifestations of COVID-19. *Life Sci.* **257**, 118063 (2020).
60. M. G. Andrews *et al.*, Tropism of SARS-CoV-2 for developing human cortical astrocytes. bioRxiv [Preprint] (2021). https://www.biorxiv.org/content/10.1101/2021.01.17.427024v1 (Accessed 18 March 2021).
61. J. Meinhardt *et al.*, Olfactory transmucosal SARS-CoV-2 invasion as a port of central nervous system entry in individuals with COVID-19. *Nat. Neurosci.* **24**, 168–175 (2021).
62. I. Alquisiras-Burgos *et al.*, Neurological complications associated with the blood-brain barrier damage induced by the inflammatory response during SARS-CoV-2 infection. *Mol. Neurobiol.* **58**, 520–535 (2021).
63. M. Hoffmann *et al.*, SARS-CoV-2 cell entry depends on ACE2 and TMPRSS2 and is blocked by a clinically proven protease inhibitor. *Cell* **181**, 271–280.e8 (2020).
64. C. Wang *et al.*, ApoE-isoform-dependent SARS-CoV-2 neurotropism and cellular response. *Cell Stem Cell* **28**, 331–342.e5 (2021).
65. A. Stukalov *et al.*, Multilevel proteomics reveals host perturbation strategies of SARS-CoV-2 and SARS-CoV. *Nature* **594**, 246–252 (2021).
66. D. Bojkova *et al.*, Proteomics of SARS-CoV-2-infected host cells reveals therapy targets. *Nature* **583**, 469–472 (2020).
67. L. Grenga *et al.*, Shotgun proteomics analysis of SARS-CoV-2-infected cells and how it can optimize whole viral particle antigen production for vaccines. *Emerg. Microbes Infect.* **9**, 1712–1721 (2020).
68. L. Pellerin, P. J. Magistretti, Sweet sixteen for ANLS. *J. Cereb. Blood Flow Metab.* **32**, 1152–1166 (2012).
69. C. Berthet *et al.*, Neuroprotective role of lactate after cerebral ischemia. *J. Cereb. Blood Flow Metab.* **29**, 1780–1789 (2009).
70. A. Suzuki *et al.*, Astrocyte-neuron lactate transport is required for long-term memory formation. *Cell* **144**, 810–823 (2011).
71. A. B. Walls *et al.*, Knockout of GAD65 has major impact on synaptic GABA synthesized from astrocyte-derived glutamine. *J. Cereb. Blood Flow Metab.* **31**, 494–503 (2011).
72. P. J. Magistretti, Role of glutamate in neuron-glia metabolic coupling. *Am. J. Clin. Nutr.* **90**, 875S–880S (2009).
73. M. Bélanger, P. J. Magistretti, The role of astroglia in neuroprotection. *Dialogues Clin. Neurosci.* **11**, 281–295 (2009).
74. M. Bélanger, I. Allaman, P. J. Magistretti, Brain energy metabolism: Focus on astrocyte-neuron metabolic cooperation. *Cell Metab.* **14**, 724–738 (2011).
75. P. Mergenthaler, U. Lindauer, G. A. Dienel, A. Meisel, Sugar for the brain: The role of glucose in physiological and pathological brain function. *Trends Neurosci.* **36**, 587–597 (2013).
76. L. K. Bak, A. Schousboe, H. S. Waagepetersen, The glutamate/GABA-glutamine cycle: Aspects of transport, neurotransmitter homeostasis and ammonia transfer. *J. Neurochem.* **98**, 641–653 (2006).
77. C. Bonansco *et al.*, Glutamate released spontaneously from astrocytes sets the threshold for synaptic plasticity. *Eur. J. Neurosci.* **33**, 1483–1492 (2011).
78. E. Guedj *et al.*, ^{18}F-FDG brain PET hypometabolism in patients with long COVID. *Eur. J. Nucl. Med. Mol. Imaging* **48**, 2823–2833 (2021).
79. E. R. Zimmer *et al.*, [^{18}F]FDG PET signal is driven by astroglial glutamate transport. *Nat. Neurosci.* **20**, 393–395 (2017).
80. S. F. Carter *et al.*, Astrocyte biomarkers in Alzheimer's disease. *Trends Mol. Med.* **25**, 77–95 (2019).
81. A. J. Stoessl, Glucose utilization: Still in the synapse. *Nat. Neurosci.* **20**, 382–384 (2017).
82. A. T. Yu, N. M. Absar, Long-term neuropsychiatric complications and 18F-FDG-PET hypometabolism in the brain from prolonged infection of COVID-19. *Alzheimer Dis. Assoc. Disord.* **36**, 173–175 (2021).
83. J. Hugon, E.-F. Msika, M. Queneau, K. Farid, C. Paquet, Long COVID: Cognitive complaints (brain fog) and dysfunction of the cingulate cortex. *J. Neurol.* **269**, 44–46 (2022).
84. I. C. Fontana, D. G. Souza, L. Pellerin, D. O. Souza, E. R. Zimmer, About the source and consequences of ^{18}F-FDG brain PET hypometabolism in short and long COVID-19. *Eur. J. Nucl. Med. Mol. Imaging* **48**, 2674–2675 (2021).
85. J. A. Hosp *et al.*, Cognitive impairment and altered cerebral glucose metabolism in the subacute stage of COVID-19. *Brain* **144**, 1263–1276 (2021).
86. K. A. Guttenplan *et al.*, Neurotoxic reactive astrocytes drive neuronal death after retinal injury. *Cell Rep.* **31**, 107776 (2020).
87. K. A. Guttenplan *et al.*, Neurotoxic reactive astrocytes induce cell death via saturated lipids. *Nature* **599**, 102–107 (2021).
88. E. Vilaplana *et al.*, Cortical microstructural correlates of astrocytosis in autosomal-dominant Alzheimer disease. *Neurology* **94**, e2026–e2036 (2020).
89. G. Vakilzadeh *et al.*, Decreased number and increased activation state of astrocytes in gray and white matter of the prefrontal cortex in autism. *Cereb. Cortex*, 10.1093/cercor/bhab523 (2022).

90. M. A. Di Biase *et al.*, Cell type-specific manifestations of cortical thickness heterogeneity in schizophrenia. *Mol. Psychiatry* **27**, 2052–2060. (2022).
91. S. Cai *et al.*, Cortical thickness differences are associated with cellular component morphogenesis of astrocytes and excitatory neurons in nonsuicidal self-injuring youth. *Cereb. Cortex*, 10.1093/cercor/bhac103 (2022).
92. C. Ecker, The neuroanatomy of autism spectrum disorder: An overview of structural neuroimaging findings and their translatability to the clinical setting. *Autism* **21**, 18–28 (2017).
93. V. T. Mensen *et al.*, Development of cortical thickness and surface area in autism spectrum disorder. *Neuroimage Clin.* **13**, 215–222 (2016).
94. M. Thom, "Epilepsy pathology" in *Encyclopedia of the Neurological Sciences*, R. B. Daroff, M. J. Aminoff, Eds. (Elsevier, 2014), pp. 136–141.
95. C. Escartin *et al.*, Reactive astrocyte nomenclature, definitions, and future directions. *Nat. Neurosci.* **24**, 312–325 (2021).
96. M. Zink, B. Vollmayr, P. J. Gebicke-Haerter, F. A. Henn, Reduced expression of glutamate transporters vGluT1, EAAT2 and EAAT4 in learned helpless rats, an animal model of depression. *Neuropharmacology* **58**, 465–473 (2010).
97. R. Kim, K. L. Healey, M. T. Sepulveda-Orengo, K. J. Reissner, Astroglial correlates of neuropsychiatric disease: From astrocytopathy to astrogliosis. *Prog. Neuropsychopharmacol. Biol. Psychiatry* **87** (Pt A), 126–146 (2018).
98. B. M. Bettcher *et al.*, Astrogliosis and episodic memory in late life: Higher GFAP is related to worse memory and white matter microstructure in healthy aging and Alzheimer's disease. *Neurobiol. Aging* **103**, 68–77 (2021).
99. F. Crunfli *et al.*, Data from "Morphological, cellular, and molecular basis of drain infection in COVID-19 patients." PRIDE partner repository. https://www.ebi.ac.uk/pride/archive?keyword=PXD023781. Deposited 25 January 2021.